

Mass Ratio of Binary Black Holes Determined from LIGO/Virgo Data Restricted to Small False Alarm Rate

Tomoya Kinugawa^{(1)(2)(3)*}, Takashi Nakamura⁽⁴⁾, and Hiroyuki Nakano⁽⁵⁾

¹Faculty of Engineering, Shinshu University, Nagano 380-8553, Japan

²Research Center for Aerospace System, Shinshu University, Nagano 380-8553, Japan

³Research Center for the Early Universe, Graduate School of Science, University of Tokyo, Tokyo 113-0033, Japan

⁴Department of Physics, Graduate School of Science, Kyoto University, Kyoto 606-8502, Japan

⁵Faculty of Law, Ryukoku University, Kyoto 612-8577, Japan

28 June 2024

ABSTRACT

We focus on gravitational-wave events of binary black-hole mergers up to the third observing run with the minimum false alarm rate smaller than 10^{-5} yr^{-1} . These events tell us that the mass ratio of two black holes follows $m_2/m_1 = 0.723$ with the chance probability of 0.00301% for the chirp mass $M_{\text{chirp}} > 18 M_{\odot}$. We show that the relation of $m_2/m_1 = 0.723$ is consistent with the binaries originated from population III stars which are the first stars in the universe. On the other hand, it is found for $M_{\text{chirp}} < 18 M_{\odot}$ that the mass ratio follows $m_2/m_1 = 0.601$ with the chance probability of 0.117% if we ignore GW190412 with $m_2/m_1 \sim 0.32$. This suggests a different origin from that for $M_{\text{chirp}} > 18 M_{\odot}$.

Key words: stars: population III, binaries: general relativity, gravitational waves, black hole mergers

1 INTRODUCTION

Possible origin of massive binary black holes (BBHs) with total mass $\sim 65 M_{\odot}$ like GW150914 which is the world's first observation of gravitational waves (GWs), is Population (Pop) III stars. Theoretically, GW events like GW150914 were predicted by Kinugawa et al. (2014) before the discovery of GW150914 by Abbott et al. (2016). After that, various compact object binaries have been observed by LIGO/Virgo GW detectors.

Many of them are BBHs (see, e.g., the third Gravitational-wave Transient Catalog (GWTC-3) of Abbott et al. (2023b)). Abbott et al. (2023a) found, e.g., the merger rate of $16\text{--}130 \text{ yr}^{-1} \text{ Gpc}^{-3}$ and the substructure in the chirp mass distribution with peak around $8 M_{\odot}$, weak structure around $15 M_{\odot}$, and peak around $30 M_{\odot}$ for the BBH events with the minimum false alarm rate (FAR), $\text{FAR}_{\text{min}} < 1 \text{ yr}^{-1}$. Here, the chirp mass M_{chirp} is defined as

$$M_{\text{chirp}} = \frac{(m_1 m_2)^{3/5}}{(m_1 + m_2)^{1/5}}, \quad (1)$$

where m_1 and m_2 ($\leq m_1$) denote the primary and secondary mass, respectively. FAR_{min} is evaluated by various pipelines used in the GW data analysis. As for the distribution of mass ratio q ,

$$q = \frac{m_2}{m_1}, \quad (2)$$

a power law was treated to model it (see, e.g., Mandel & Broekgaarden (2022) for rates of compact object coalescences, and references therein).

In the following, we focus only on BBHs, and especially the masses¹. Although the mass ratio of binaries is estimated less accurately than the chirp mass, we can find several studies on the mass ratio related to Abbott et al. (2023a). Tiwari (2022) showed that there is no prominent dependence either on the chirp mass or the aligned spin in the mass ratio distribution from the 69 GW events with $\text{FAR}_{\text{min}} < 1 \text{ yr}^{-1}$. Here, it should be noted that the estimation of spins is more difficult than the mass ratio. In our galaxy, Wagg et al. (2022) give a prediction of the mass ratio distribution with a peak at $q \approx 0.4$ for BBHs observed by a 4 yr LISA observation (Amaro-Seoane et al. 2017) in their fiducial model. In simulations for hierarchical triples from low-mass young star clusters, Trani et al. (2022) found $q \approx 0.3$ which is lower than that from binaries (see, e.g., Rastello et al. (2021)). Broekgaarden et al. (2022a) showed that at least 95% of BBH mergers detectable by LIGO/Virgo/KAGRA (LVK) detector network at design sensitivity have $q \gtrsim 0.25$ in their 560 models. Stegmann et al. (2022b) presented orbital properties

¹ There are also studies on the spins, for example, see Fishbach et al. (2022) for limits on hierarchical BH mergers from an effective inspiral spin parameter. To extract more detailed information of spins, we will require multiband GW observations (Isoyama et al. 2018) with a decihertz GW detector, B-DECIGO (Nakamura et al. 2016).

* E-mail: kinugawa@shinshu-u.ac.jp

(masses, mass ratio, eccentricity, orbital separation etc.) of surviving systems after a BBH has formed in the inner binary and those of BBHs which are formed from an isolated binary population for metallicities, $Z = 0.01 Z_{\odot}$ and Z_{\odot} , where Z_{\odot} is the solar metallicity, obtained by using a new triple stellar evolution code. Using the 69 GW events with $\text{FAR}_{\text{min}} < 1 \text{ yr}^{-1}$, Li et al. (2022) found that the observed BBHs have a much stronger preference for equal mass binaries in their parameterized primary-mass distribution models. Using direct N -body simulations for star cluster models, Chattopadhyay et al. (2022) found that the distributions of the mass ratio have median values in the range of 0.8–0.9 (except for one model). Mould et al. (2022a) have prepared a deep-learning pipeline to constrain properties of hierarchical black-hole mergers. In the field of galaxies, Stegmann et al. (2022a) discussed BBHs starting from hierarchical triple population and isolated binary population, and found that the observed lower mass ratio ($q \lesssim 0.5$) BBHs can be explained by the contribution from the outer binary channel of the triple population. In mass-ratio reversal systems where the second BH to form in the binary are more massive than the first BH, Broekgaarden et al. (2022b) found that BBHs with $M_{\text{chirp}} \gtrsim 10 M_{\odot}$ and $q \gtrsim 0.6$ are dominant in the GW observation (see also Mould et al. (2022b)). Briel et al. (2023) introduced super-Eddington accretion into a population synthesis code. Antonini et al. (2023) discussed a scenario of merging BBHs which are formed dynamically in globular clusters, and found that the observed events shown in GWTC-3 cannot be explained in the above scenario (see also Mahapatra et al. (2022)). In Franciolini et al. (2022); Escriva et al. (2023), the mass ratio has been discussed by treating a varying equation of state at the QCD epoch in primordial BH formation scenario (see also Carr et al. (2023) for a recent review on primordial BHs). Edelman et al. (2023) have suggested some possible plateaus at several mass ratios in the distribution by using a data-driven, non-parametric model. Oh et al. (2023) have discussed merging compact binaries with highly asymmetric mass ratios, and found that a natal kick of $\sim 250 \text{ km/s}$ is required for systems with $q \lesssim 0.1$ to merge. Costa et al. (2023) discussed BBHs from Pop II ($Z = 10^{-4}$) and III ($Z = 10^{-11}$) stars in their models, and found that the mass ratios for Pop II BBHs are almost $q \sim 1$ and the peak of mass ratios for Pop III BBHs is $q = 0.8 - 0.9$ in most of their models. In Santoliquido et al. (2023), the redshift dependence of mass ratio of Pop III BBHs was presented. In their models, Pop III BBHs merging at low redshift ($z \leq 4$) have low mass ratios, $q \approx 0.5 - 0.7$ (the median values), while typically $q \sim 0.9$ at high redshift. For star clusters, Arca Sedda et al. (2023b) have investigated dependence of the host cluster structure and the physics of massive star evolution by using their database which has 19 direct N -body models to discuss various types of compact binary mergers (Arca Sedda et al. 2023a), and found $q > 0.6$ and $m_1/M_{\odot} = 5-40$ in primordial binary systems, and $q = 0.6-1$ for $m_1 < 15 M_{\odot}$, $q > 0.9$ for $15 M_{\odot} < m_1 < 40.5 M_{\odot}$ and $q > 0.7$ for $40.5 M_{\odot} < m_1$ in dynamical mergers.

2 ANALYSIS OF DATA WITH SMALL FALSE ALARM RATE

The GW events with $\text{FAR}_{\text{min}} < 1 \times 10^{-5} \text{ yr}^{-1}$ in Abbott et al. (2023a) are summarized in Table 1 (note that because there are some updates during this work, we use the latest ones from the online GWTC (The LIGO Scientific Collaboration et al. 2023)). The reason for this restriction of FAR is that we treat more accurate tendency of the events. Here, we show the event name, primary mass m_1 , secondary mass m_2 , chirp mass M_{chirp} , luminosity distance D_L , and mass ratio q . BNS, NS-BH, MGCO-BH, and BBH in the column of “Binary type” mean binary neutron star, neutron star-black hole binary, mass-gap compact object²-black hole binary, and binary black hole, respectively.

The study by Kinugawa et al. (2020) is based on our old code developed by Kinugawa et al. (2014) for population synthesis simulations of the evolution of Pop III stars. There are, however, at least two big differences between the two papers. The first one is that the star formation rate (SFR) of Pop III stars is a factor 3 decreased due to the new observational data of CMB (Cosmic Microwave Background). The second one is the number of simulated models. In Kinugawa et al. (2014), only two models with different initial mass function (IMF) are simulated, while in Kinugawa et al. (2020) seven models with different IMF, initial mass ratio, initial separation, initial eccentricity, mass transfer rate, accretion fraction (β), common envelope parameter $\alpha\lambda$ and tidal coefficient factor (E) are simulated.

In our previous study (Kinugawa et al. 2021b), we found a very simple relation, $m_2 \simeq 0.7 m_1$ ³ for BBHs with $M_{\text{chirp}} \gtrsim 20 M_{\odot}$ summarized in GWTC-2 (Abbott et al. 2021), and that this relation is consistent with the mass distribution in our 6 population synthesis simulations of Pop III stars in Fig. 4 of Kinugawa et al. (2021b). Therefore, first, we focus only on 20 BBH events with $M_{\text{chirp}} > 18 M_{\odot}$. This is because there exists a small gap in the chirp mass between GW190512_180714 and GW191215_223052. Figure 1 shows m_1 and m_2 of these events. Assuming $m_2 = 0$ at $m_1 = 0$, the linear fitting function is obtained as

$$m_2 = 0.723 m_1, \quad (3)$$

and the correlation coefficient is 0.933 with the chance probability of 0.00301%.

Next, we treat the remaining BBH events. Figure 2 shows m_1 and m_2 of 13 BBH events with $M_{\text{chirp}} < 18 M_{\odot}$ given in Table 1. Here, we have ignored GW190814_211039 which has a MGCO in the binary. Assuming $m_2 = 0$ at $m_1 = 0$, the linear fitting function is obtained as $m_2 = 0.527 m_1$, and the correlation coefficient is 0.741. The correlation between the data and this fitting function is not so high.

Here, we note that GW190412_053044 has large unequal component masses (Abbott et al. 2020b). As an alternative interpretation of masses for this GW event, we may have $q = 0.31^{+0.05}_{-0.04}$ from a prior with a non-spinning primary and a rapidly spinning secondary (Mandel & Fragos 2020) (see also Kinugawa et al. (2020)). Also, Zevin et al. (2020) found

² The mass of MGCOs lies in 2–5 M_{\odot} . See Kinugawa et al. (2021c) for details.

³ Broadhurst et al. (2022) also mentioned this relation for nearly all BBH GW events.

Table 1. Event name (the YYMMDD_hhmmss format), primary mass m_1 , secondary mass m_2 , chirp mass M_{chirp} in unit of the solar mass, M_{\odot} , and luminosity distance D_L [Mpc] from [The LIGO Scientific Collaboration et al. \(2023\)](#). These are expressed by the median and 90%-symmetric credible interval. The mass ratio q is evaluated by using the median values of m_1 and m_2 . Binary type shows binary neutron star (BNS), neutron star-black hole binary (NS-BH), mass-gap compact object-black hole binary (MGCO-BH), or binary black hole (BBH). Here, we focus only on events with $\mathbf{FAR}_{\text{min}} < 1 \times 10^{-5} \text{ yr}^{-1}$ where $\mathbf{FAR}_{\text{min}}$ means the minimum FAR evaluated by various GW data analyses. These events have the probability of astrophysical (signal) origin, $p_{\text{astro}} > 0.99$. The data are sorted by M_{chirp} . The first 2 events are BNSs and NS-BH binaries. The next 14 events are BBHs and a MGCO-BH, and have $M_{\text{chirp}} < 18 M_{\odot}$, and the final 20 events are BBHs and have $M_{\text{chirp}} > 18 M_{\odot}$.

Event name	m_1	m_2	M_{chirp}	D_L	q	Binary type
GW170817	$1.46^{+0.12}_{-0.1}$	$1.27^{+0.09}_{-0.09}$	$1.186^{+0.001}_{-0.001}$	40^{+7}_{-15}	0.87	BNS
GW200115_042309	$5.9^{+2}_{-2.5}$	$1.44^{+0.85}_{-0.29}$	$2.43^{+0.05}_{-0.07}$	290^{+150}_{-100}	0.24	NS-BH
GW190924_021846	$8.8^{+4.3}_{-1.8}$	$5.1^{+1.2}_{-1.5}$	$5.8^{+0.2}_{-0.2}$	550^{+220}_{-220}	0.58	BBH
GW190814_211039	$23.3^{+1.4}_{-1.4}$	$2.6^{+0.1}_{-0.1}$	$6.11^{+0.06}_{-0.05}$	230^{+40}_{-50}	0.11	MGCO-BH
GW191129_134029	$10.7^{+4.1}_{-2.1}$	$6.7^{+1.5}_{-1.7}$	$7.31^{+0.43}_{-0.28}$	790^{+260}_{-330}	0.63	BBH
GW200202_154313	$10.1^{+3.5}_{-1.4}$	$7.3^{+1.1}_{-1.7}$	$7.49^{+0.24}_{-0.2}$	410^{+150}_{-160}	0.72	BBH
GW170608	$11^{+5.5}_{-1.7}$	$7.6^{+1.4}_{-2.2}$	$7.9^{+0.2}_{-0.2}$	320^{+120}_{-110}	0.69	BBH
GW191216_213338	$12.1^{+4.6}_{-2.3}$	$7.7^{+1.6}_{-1.9}$	$8.33^{+0.22}_{-0.19}$	340^{+120}_{-130}	0.64	BBH
GW190707_093326	$12.1^{+2.6}_{-2}$	$7.9^{+1.6}_{-1.3}$	$8.4^{+0.6}_{-0.4}$	850^{+340}_{-400}	0.65	BBH
GW191204_171526	$11.9^{+3.3}_{-1.8}$	$8.2^{+1.4}_{-1.6}$	$8.55^{+0.38}_{-0.27}$	650^{+190}_{-250}	0.69	BBH
GW190728_064510	$12.5^{+6.9}_{-2.3}$	$8^{+1.7}_{-2.6}$	$8.6^{+0.6}_{-0.3}$	880^{+260}_{-380}	0.64	BBH
GW200316_215756	$13.1^{+10.2}_{-2.9}$	$7.8^{+1.9}_{-2.9}$	$8.75^{+0.62}_{-0.55}$	1120^{+470}_{-440}	0.60	BBH
GW151226	$13.7^{+8.8}_{-3.2}$	$7.7^{+2.2}_{-2.5}$	$8.9^{+0.3}_{-0.3}$	450^{+180}_{-190}	0.56	BBH
GW190720_000836	$14.2^{+5.6}_{-3.3}$	$7.5^{+2.2}_{-1.8}$	$9^{+0.4}_{-0.8}$	770^{+650}_{-260}	0.53	BBH
GW190412_053044	27.7^{+6}_{-6}	$9^{+2}_{-1.4}$	$13.3^{+0.5}_{-0.5}$	720^{+240}_{-220}	0.32	BBH
GW190512_180714	$23.2^{+5.6}_{-5.6}$	$12.5^{+3.5}_{-2.6}$	$14.6^{+1.4}_{-0.9}$	1460^{+510}_{-590}	0.54	BBH
GW191215_223052	$24.9^{+7.1}_{-4.1}$	$18.1^{+3.8}_{-4.1}$	$18.4^{+2.2}_{-1.7}$	1930^{+890}_{-860}	0.73	BBH
GW190408_181802	$24.8^{+5.4}_{-3.5}$	$18.5^{+3.3}_{-4}$	$18.5^{+1.9}_{-1.2}$	1540^{+440}_{-620}	0.75	BBH
GW170104	$30.8^{+7.3}_{-5.6}$	$20^{+4.9}_{-4.6}$	$21.4^{+2.2}_{-1.8}$	990^{+440}_{-430}	0.65	BBH
GW170814	$30.6^{+5.6}_{-3}$	$25.2^{+2.8}_{-4}$	$24.1^{+1.4}_{-1.1}$	600^{+150}_{-220}	0.82	BBH
GW190915_235702	$32.6^{+8.8}_{-4.9}$	$24.5^{+4.9}_{-5.8}$	$24.4^{+3}_{-2.3}$	1750^{+710}_{-650}	0.75	BBH
GW190828_063405	$31.9^{+5.4}_{-4.1}$	$25.8^{+4.9}_{-5.3}$	$24.6^{+3.6}_{-2}$	2070^{+650}_{-920}	0.81	BBH
GW170809	$35^{+8.3}_{-5.9}$	$23.8^{+5.1}_{-5.2}$	$24.9^{+2.1}_{-1.7}$	1030^{+320}_{-390}	0.68	BBH
GW190630_185205	$35.1^{+6.5}_{-5.5}$	$24^{+5.5}_{-5.2}$	$25.1^{+2.2}_{-2.1}$	870^{+530}_{-360}	0.68	BBH
GW200311_115853	$34.2^{+6.4}_{-3.8}$	$27.7^{+4.1}_{-5.9}$	$26.6^{+2.4}_{-2}$	1170^{+280}_{-400}	0.81	BBH
GW200129_065458	$34.5^{+9.9}_{-3.2}$	$28.9^{+3.4}_{-9.3}$	$27.2^{+2.1}_{-2.3}$	900^{+290}_{-380}	0.84	BBH
GW200112_155838	$35.6^{+6.7}_{-4.5}$	$28.3^{+4.4}_{-5.9}$	$27.4^{+2.6}_{-2.1}$	1250^{+430}_{-460}	0.79	BBH
GW150914	$35.6^{+4.7}_{-3.1}$	$30.6^{+3}_{-4.4}$	$28.6^{+1.7}_{-1.5}$	440^{+150}_{-170}	0.86	BBH
GW170823	$39.5^{+11.2}_{-6.7}$	$29^{+6.7}_{-7.8}$	$29.2^{+4.6}_{-3.6}$	1940^{+970}_{-900}	0.73	BBH
GW190503_185404	$41.3^{+10.3}_{-7.7}$	$28.3^{+7.5}_{-9.2}$	$29.3^{+4.5}_{-4.4}$	1520^{+630}_{-600}	0.69	BBH
GW190727_060333	$38.9^{+8.9}_{-6}$	$30.2^{+6.5}_{-8.3}$	$29.4^{+4.6}_{-3.7}$	3070^{+1300}_{-1230}	0.78	BBH
GW200224_222234	$40^{+6.9}_{-4.5}$	$32.5^{+5}_{-7.2}$	$31.1^{+3.2}_{-2.6}$	1710^{+490}_{-640}	0.81	BBH
GW190521_074359	$43.4^{+5.8}_{-5.5}$	$33.4^{+3.2}_{-6.8}$	$32.8^{+3.2}_{-2.8}$	1080^{+580}_{-530}	0.77	BBH
GW191222_033537	$45.1^{+10.9}_{-8}$	$34.7^{+9.3}_{-10.5}$	$33.8^{+7.1}_{-5}$	3000^{+1700}_{-1700}	0.77	BBH
GW190519_153544	$65.1^{+10.8}_{-11}$	$40.8^{+11.5}_{-12.7}$	$44.3^{+6.8}_{-7.5}$	2600^{+1720}_{-960}	0.63	BBH
GW190602_175927	$71.8^{+18.1}_{-14.6}$	$44.8^{+15.5}_{-19.6}$	$48^{+9.5}_{-9.7}$	2840^{+1930}_{-1280}	0.62	BBH

$q \lesssim 0.57$ in the 99% credible level from various models. Interestingly, although the GW data did not prefer Model G with a prior assumption, $\chi_1 = \chi_2 = 0$ in the above paper, this model gave $q \approx 0.55$. [Antonelli et al. \(2023\)](#) have also discussed the most likely formation channel. When we ignore this GW190412_053044 event in the analysis of mass ratio, the fitting is improved as Fig. 3. Assuming $m_2 = 0$ at $m_1 = 0$,

the linear fitting function is obtained as

$$m_2 = 0.601 m_1, \quad (4)$$

and the correlation coefficient becomes 0.937 with the chance probability of 0.117%. To argue the origin of BBH events for $M_{\text{chirp}} < 18 M_{\odot}$, we need more examples of BBHs similar to GW190412_053044 in the near future by the O4 Observing run ([Abbott et al. 2020a](#)).

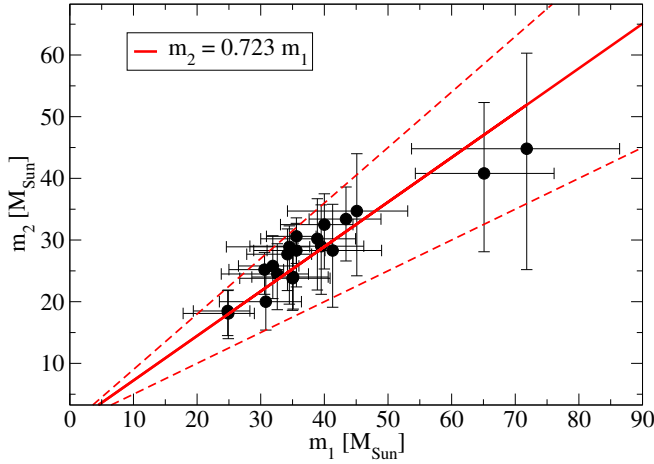


Figure 1. 20 BBH events with $M_{\text{chirp}} > 18 M_{\odot}$ in Table 1. We present the median and 90%-symmetric credible interval for m_1 and m_2 . The fitting (the solid red line) gives $m_2 = 0.723 m_1$, and the correlation coefficient is 0.933 with the chance probability of 0.00301%. As references, we show $m_2 = 0.5 m_1$ and $m_2 = 0.9 m_1$ as the dashed red lines.

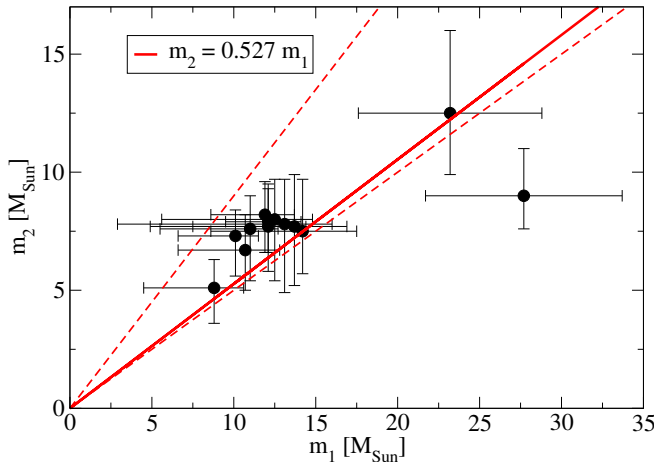


Figure 2. 13 BBH events with $M_{\text{chirp}} < 18 M_{\odot}$ in Table 1. We present the median and 90%-symmetric credible interval for m_1 and m_2 . The fitting (the solid red line) gives $m_2 = 0.527 m_1$, and the correlation coefficient is 0.741. As references, we show $m_2 = 0.5 m_1$ and $m_2 = 0.9 m_1$ as the dashed red lines.

In Kinugawa et al. (2020, 2021b), we performed 10^6 Pop III binary evolution by using 12 different models with initial conditions of mass function, mass ratio, separation, and eccentricity as well as physical models (see Tables 2 and 3 of Kinugawa et al. (2020) and Section 2.2 of Kinugawa et al. (2021b) for details of each model). These Pop III binary population synthesis calculations are based on the Pop III stellar evolution model of Marigo et al. (2001). The fiducial model of Kinugawa et al. (2020) assumes the flat IMF from $10 M_{\odot}$ to $150 M_{\odot}$, the flat mass ratio distribution from $10 M_{\odot}/M_1$ to 1, the logflat separation distribution, and the eccentricity distribution proportional to e for determination of initial Pop III binary conditions. In regards to binary evolution, the fiducial model of Kinugawa et al. (2020) uses the common envelope parameter $\alpha\lambda = 1$, the conservative mass transfer,

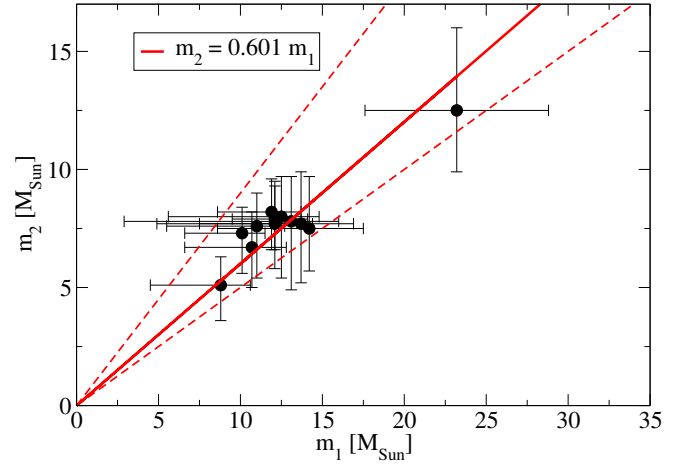


Figure 3. 12 BBH events with $M_{\text{chirp}} < 18 M_{\odot}$ in Table 1. We present the median and 90%-symmetric credible interval for m_1 and m_2 . Here, we have ignored a BBH event, GW190412_053044. The fitting (the solid red line) gives $m_2 = 0.601 m_1$, and the correlation coefficient is 0.937 with the chance probability of 0.117%. As references, we show $m_2 = 0.5 m_1$ and $m_2 = 0.9 m_1$ as the dashed red lines.

and no BH natal kick. The al01 model of Kinugawa et al. (2020) uses the same initial distributions and binary parameters of the fiducial model, except for the common envelope parameter $\alpha\lambda = 0.1$. The MT05 model of Kinugawa et al. (2020) also uses the same initial distributions and binary parameters except for the unconservative mass transfer which loses half of accreted mass. The M100 model of Kinugawa et al. (2020) has modified the initial primary star mass range from $10 M_{\odot}$ to $100 M_{\odot}$ compared to the fiducial model. The K14 model of Kinugawa et al. (2020) is based on our first Pop III calculation (Kinugawa et al. 2014). Although this model uses the same initial distribution and binary parameters as the M100 model, the main difference between the two models is the treatment of the mass transfer rate in the stable Roche lobe overflow shown from Eq. (4) to Eq. (7) of Kinugawa et al. (2020) in details. The FS1 and FS2 models of Kinugawa et al. (2020) use the initial distribution and the binary parameters of FS1 and FS2 models in Belczynski et al. (2017), but the Pop III stellar evolution and equations of binary evolution are the same as the fiducial model of Kinugawa et al. (2020). The flat model of Kinugawa et al. (2021b) is same as the M100 model of Kinugawa et al. (2020). The M-05, M-1, M-15, M-2, and Sal models of Kinugawa et al. (2021b) use the $f(M_1) \propto M_1^{-0.5}, M_1^{-1.0}, M_1^{-1.5}, M_1^{-2}$ and Salpeter IMF, respectively. These models use the same initial conditions and binary parameters of the flat model of Kinugawa et al. (2021b) (M100 model of Kinugawa et al. (2020)) except for IMF.

Figures 4 and 5 show the chirp-mass distribution of 20 BBH events with $M_{\text{chirp}} > 18 M_{\odot}$. Figure 4 compares the GW result and models of Kinugawa et al. (2020). The vertical axis shows the expected number of BBHs for a given range of M_{chirp} so that the total number should be 20. The filled (red) circles show the observed 20 GW events, and the filled (purple) triangles, filled (copper) triangles, filled (mustard) triangles, filled (khaki) triangles, filled (light blue) diamonds, filled (blue) squares, and (green) asterisks denote the results

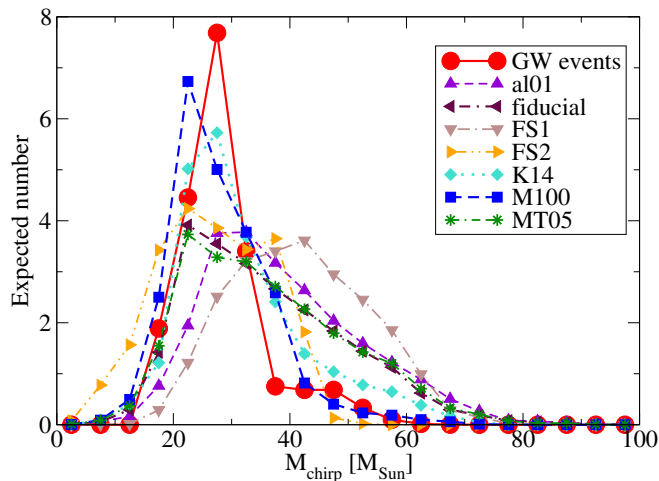


Figure 4. Chirp-mass distribution of 20 BBH events with $M_{\text{chirp}} > 18 M_{\odot}$ for Kinugawa et al. (2020). The ordinate shows the expected number of BBH for given range of M_{chirp} so that the total number should be 20. The filled (red) circles show the observed 20 GW events, and the filled (purple) triangles, filled (copper) triangles, filled (mustard) triangles, filled (khaki) triangles, filled (light blue) squares, filled (blue) squares, and filled (green) asterisks denote the results of the al01, fiducial, FS1, FS2, K14, M100 and MT05 models by assuming that the total observable number is 20.

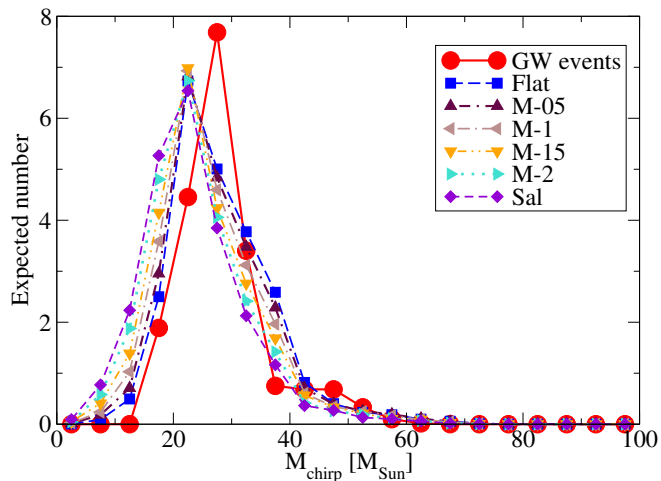


Figure 5. Same figure of Fig. 4 but for Kinugawa et al. (2021b). The filled (red) circles show the observed 20 GW events, and the filled (blue) squares, filled (copper) triangles, filled (mustard) triangles, filled (khaki) triangles, filled (light blue) triangles, and filled (purple) diamonds denote the results of the Flat, M-05, M-1, M-15, M-2, and Sal models by assuming the total observable number is 20.

of the al01, fiducial, FS1, FS2, K14, M100 and MT05 models by assuming the total observable number is 20. We can see that both the M100 and K14 models fit well with the observed one shown by the filled (red) circles.

Figure 5 compares the GW result and models of Kinugawa et al. (2021b). The vertical axis shows the expected number of BBHs for a given range of M_{chirp} so that the total number should be 20. The filled (red) circles show the observed

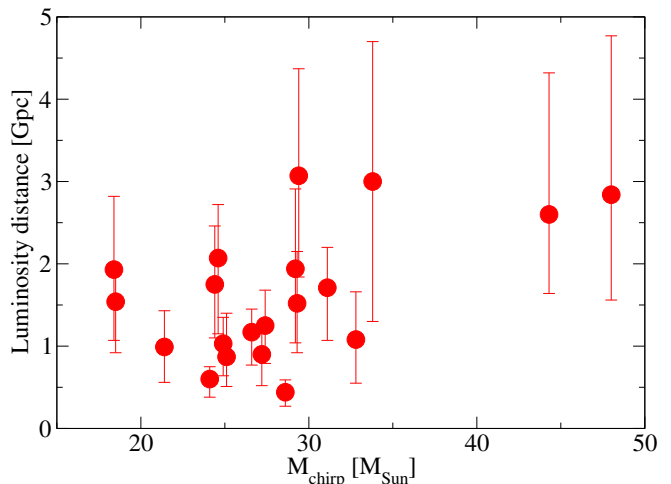


Figure 6. Luminosity distance (D_L) vs. chirp-mass of 20 BBH events with $M_{\text{chirp}} > 18 M_{\odot}$. Here, we present only the median of the chirp mass, and the median and 90%-symmetric credible interval of the luminosity distance.

20 GW events, and the filled (blue) squares, filled (copper) triangles, filled (mustard) triangles, filled (khaki) triangles, filled (light blue) triangles, and filled (purple) diamonds denote the results of the Flat, M-05, M-1, M-15, M-2, Sal models by assuming the total observable number is 20. We can see that all models of Kinugawa et al. (2021b) have almost same shape and fit well with the observed one shown by the filled (red) circles.

In Fig. 4, K14 and M100 models seem to match the data, while the other models are not suitable. In Fig. 5, all models appear to match the data. In other words, there are currently too many models that seem to be consistent with observations. This is because the current number of observations is too low. The only solution is to increase the number of observations by two or three times. Figures 4 and 5 suggest that, in order to match with observational results, it is crucial to have an initial mass range below $100 M_{\odot}$ rather than focusing on the initial distribution, binary parameters, or the initial mass function (IMF). Note that Kinugawa et al. (2020) did not account for the effects of pair-instability supernovae (PPISN). Considering PPISN, primary stars with initial masses above $100 M_{\odot}$ lose mass due to PPISN, reducing their mass to around $30\text{--}50 M_{\odot}$ (Kinugawa et al. 2021a). This effect might lead to a reduction in the number of higher-mass black holes on the heavy side of the black hole mass distribution in models considering initial masses above $100 M_{\odot}$, making them more consistent with observations.

Figure 6 shows the luminosity distance (D_L) distribution of 20 observed BBH events. We see that $D_L \lesssim 3 \text{ Gpc}$ for $M_{\text{chirp}} \lesssim 30 M_{\odot}$ while $D_L \gtrsim 1.5 \text{ Gpc}$ for $M_{\text{chirp}} \gtrsim 30 M_{\odot}$. But the errors are still large to say the above facts definitely.

3 DISCUSSION

Figures 7 and 8 show the delay time (T_{delay}) distributions for each mass ratio of merging Pop III BBHs in the M100 and K14 models, respectively. We present the delay time distributions of Pop III BBHs which merge within the Hubble

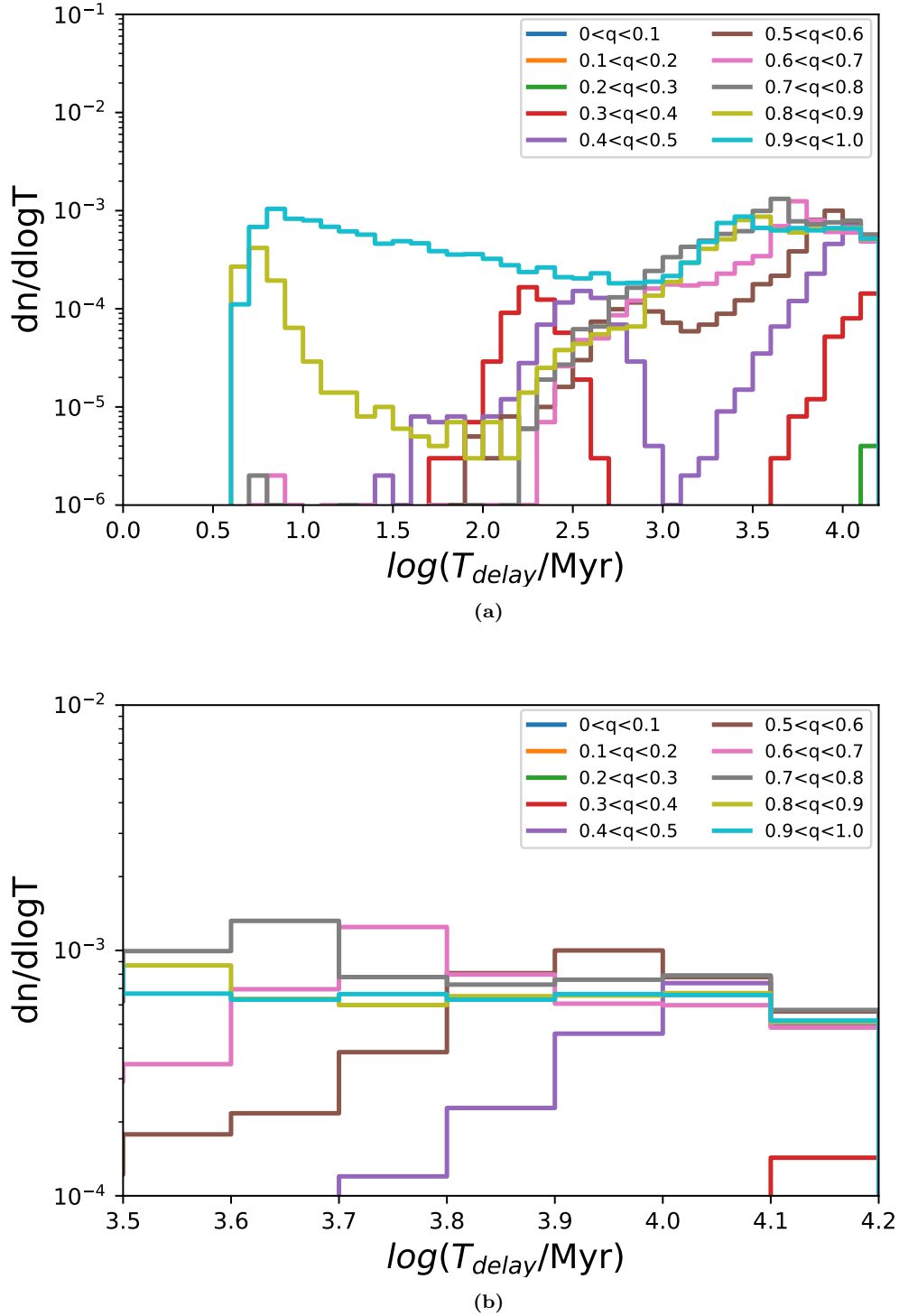


Figure 7. Delay time (T_{delay}) distributions for each mass ratio of merging Pop III BBHs in the M100 model. The distribution is normalized by the number of total Pop III binaries. (a) shows the delay time distributions of BBHs which merge within the Hubble time. (b) shows the delay time distributions of BBHs of which the merger time is more than $10^{3.5}$ Myrs and less than the Hubble time.

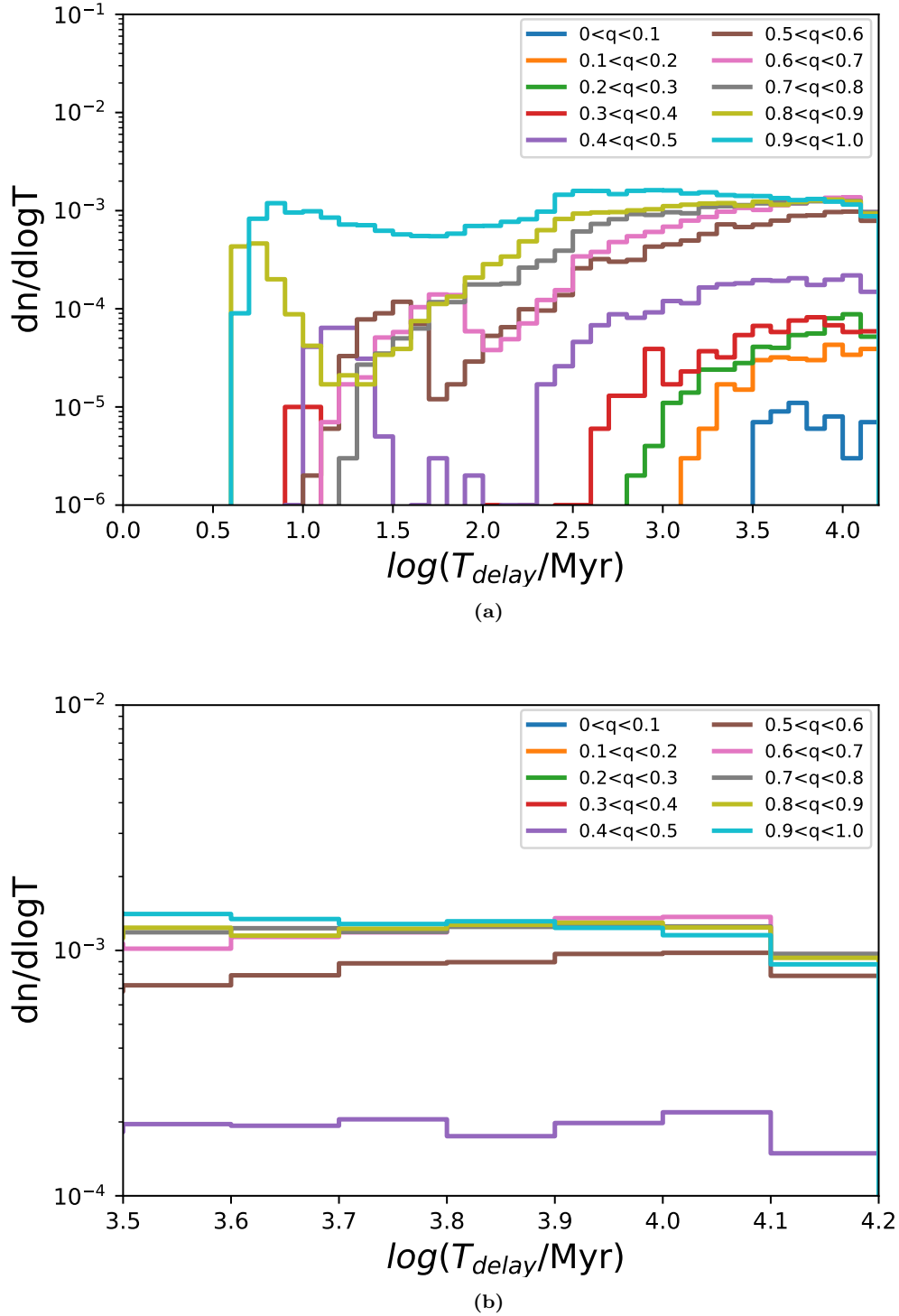


Figure 8. Same figure of Fig. 7 but for the K14 model.

time in Figs. 7a and 8a, while the delay time distributions of Pop III BBHs of which the merger time is more than $10^{3.5}$ Myrs and less than the Hubble time in Figs. 7b and 8b. These distributions are normalized by the number of total Pop III binaries.

It is found in Figs. 7a and 8a that the nearly equal-mass

BBH mergers predominate in a very short delay time region ($T_{\text{delay}} \lesssim 100$ Myrs). In other words, the nearly equal-mass Pop III BBH mergers predominate in the very early universe ($z \gtrsim 10$) since the Pop III stars are born and died at high redshift ($z \gtrsim 10$). These BBH mergers at the high redshift can be observed future GW observatory such as the Ein-

stein telescope (ET) (Hild et al. 2011), the Cosmic Explorer (CE) (Evans et al. 2021), and DECIGO (Seto et al. 2001; Nakamura et al. 2016).

The formation channel is the reason why the equal mass Pop III BBHs merge at the high redshift. In our previous paper (Kinugawa et al. 2020), we classified the Pop III BBH formation channel into the 5 channels such as NoCE, $1CE_P$, $1CE_S$, $1CE_D$, and 2CE. NoCE means that Pop III BBHs evolve not via a common envelope phase. $1CE_P$, $1CE_S$, and $1CE_D$ are Pop III BBHs evolved via one common envelope phase caused by the primary giant star, the secondary giant star, or double giant stars, respectively. 2CE is the Pop III BBHs experienced more than two common envelope phases. Figure 5 of Kinugawa et al. (2020) shows that almost all Pop III BBHs merging with very short delay time ($T_{\text{delay}} \lesssim 100$ Myrs) evolved via the $1CE_D$ channel.

Figure 9 shows an example of $1CE_D$ channel. Pop III binaries of which initial masses are nearly equal tend to evolve via the $1CE_D$ channel. If the initial masses of a binary are similar, the timescale of evolution is similar as well. Therefore, they both become giant stars at almost the same time and shed their envelopes simultaneously through a double common envelope process. A significant amount of orbital energy is also lost by shedding the outer envelopes of both stars. After that, a very close binary He star tends to remain, and they can become a close BBH which merges within 100 Myrs.

Next, we focus on Figs. 7b and 8b where Pop III BBHs with a long delay time are presented for each mass ratio. Figures 10 and 11 show the mass ratio distributions of merging Pop III BBHs of which delay time is more than $10^{3.5}$ Myrs and less than the Hubble time for M100 and K14 models, respectively. These BBHs can be detected within the detection range of LVK collaboration.

In the M100 model, the main contribution to the mass ratio distribution is the $1CE_P$ channel. Subdominant ones are NoCE and 2CE channels. These channels make BBHs with various mass ratios from 0.4 to 1, unlike the $1CE_D$ channel. In the K14 model, the main contribution is the NoCE channel. Subdominant ones are $1CE_P$ and 2CE channels. This model also has various mass ratio BBH mergers with a long delay time like the M100 model.

4 SUMMARY AND CONCLUSION

In this paper, we focus on gravitational-wave events of binary black-hole mergers up to the third observing run with the minimum false alarm rate smaller than 10^{-5} yr^{-1} . These events tell us that the mass ratio of two black holes follows $m_2/m_1 = 0.723$ with the chance probability of 0.00301% for $M_{\text{chirp}} > 18 M_{\odot}$ where M_{chirp} is called the chirp mass of binary. We show that the relation of $m_2/m_1 = 0.723$ is consistent with the binaries originated from Pop III stars which are the first stars in the universe.

On the other hand, it is found for $M_{\text{chirp}} < 18 M_{\odot}$ that the mass ratio follows $m_2/m_1 = 0.601$ with the chance probability of 0.117% if we ignore GW190412 with $m_2/m_1 \sim 0.32$. This suggests a different origin from that for $M_{\text{chirp}} > 18 M_{\odot}$. For $M_{\text{chirp}} < 18 M_{\odot}$, there is one with significantly different m_2/m_1 , and the correspondence to Pop I and Pop II is not clear. To state anything conclusively, the number of observed

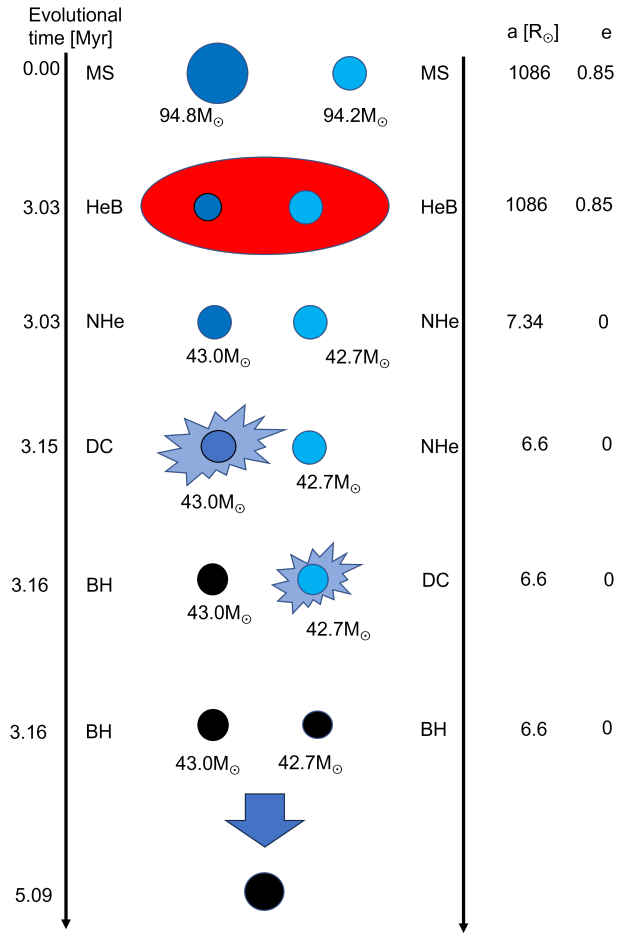


Figure 9. Example of Pop III binary evolution via $1CE_D$ channel. Here, a and e denote the separation and eccentricity, respectively. MS, HeB, NHe, DC and BH mean main-sequence phase, helium-burning phase, naked helium star, degenerate core, and black hole, respectively.

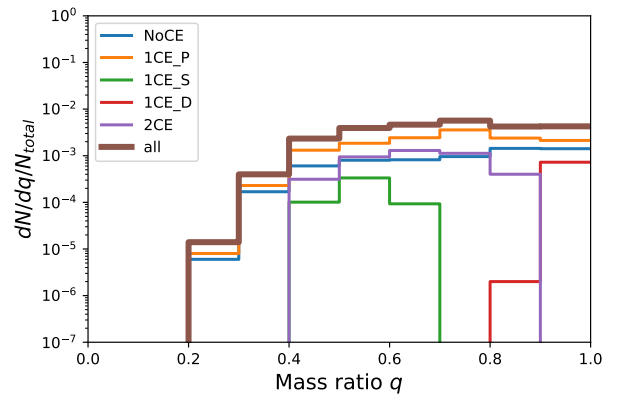


Figure 10. Mass ratio distributions of merging Pop III BBHs of which delay time is more than $10^{3.5}$ Myrs and less than the Hubble time for M100 model.

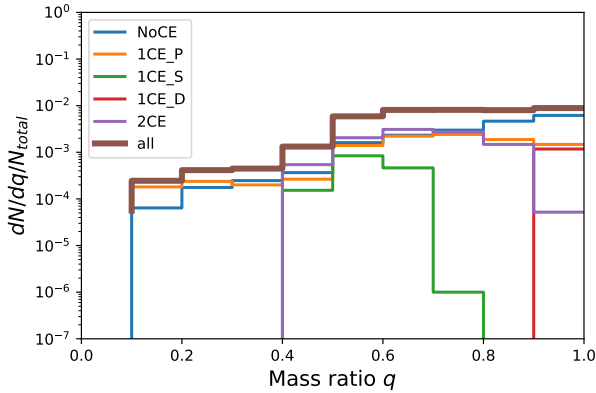


Figure 11. Same figure of Fig. 10 but for the K14 model.

events needs to increase by several times. Also, in future observations, events with higher redshifts will become visible.

Furthermore, according to Figs. 7, 8, 10 and 11, it is expected that observations at high redshift, unlike observations at low redshift, would exhibit a higher proportion of equal-mass BBH mergers. A comparison between the low-redshift results from the current ground-based GW observations and the high-redshift results from future observations such as ET, CE and DECIGO enables us to check the Pop III origin model.

ACKNOWLEDGMENT

T. K. acknowledges support from JSPS KAKENHI Grant Numbers JP21K13915 and JP22K03630. H. N. acknowledges support from JSPS KAKENHI Grant Numbers JP21H01082, JP21K03582 and JP23K03432, and also would like to thank to Y. W. for her hospitality.

DATA AVAILABILITY

Results will be shared on reasonable request to the corresponding author.

REFERENCES

Abbott B. P., et al., 2016, *Physical Review Letters*, **116**, 061102
 Abbott B. P., et al., 2020a, *Living Reviews in Relativity*, **23**, 3
 Abbott R., et al., 2020b, *Phys. Rev. D*, **102**, 043015
 Abbott R., et al., 2021, *Physical Review X*, **11**, 021053
 Abbott R., et al., 2023a, *Physical Review X*, **13**, 011048
 Abbott R., et al., 2023b, *Physical Review X*, **13**, 041039
 Amaro-Seoane P., et al., 2017, arXiv e-prints, p. arXiv:1702.00786
 Antonelli A., Kritos K., Ng K. K. Y., Cotesta R., Berti E., 2023, *Phys. Rev. D*, **108**, 084044
 Antonini F., Gieles M., Dosopoulou F., Chattopadhyay D., 2023, *MNRAS*, **522**, 466
 Arca Sedda M., et al., 2023a, arXiv e-prints, p. arXiv:2307.04805
 Arca Sedda M., Kamlah A. W. H., Spurzem R., Rizzuto F. P., Giersz M., Naab T., Berczik P., 2023b, arXiv e-prints, p. arXiv:2307.04807

Belczynski K., Ryu T., Perna R., Berti E., Tanaka T. L., Bulik T., 2017, *MNRAS*, **471**, 4702
 Briel M. M., Stevance H. F., Eldridge J. J., 2023, *MNRAS*, **520**, 5724
 Broadhurst T., Diego J. M., Smoot G. F., 2022, arXiv e-prints, p. arXiv:2202.05861
 Broekgaarden F. S., et al., 2022a, *MNRAS*, **516**, 5737
 Broekgaarden F. S., Stevenson S., Thrane E., 2022b, *ApJ*, **938**, 45
 Carr B., Clesse S., Garcia-Bellido J., Hawkins M., Kuhnel F., 2023, arXiv e-prints, p. arXiv:2306.03903
 Chattopadhyay D., Hurley J., Stevenson S., Raidani A., 2022, *MNRAS*, **513**, 4527
 Costa G., Mapelli M., Iorio G., Santoliquido F., Escobar G. J., Klessen R. S., Bressan A., 2023, *MNRAS*, **525**, 2891
 Edelman B., Farr B., Doctor Z., 2023, *ApJ*, **946**, 16
 Escriva A., Bagui E., Clesse S., 2023, *J. Cosmology Astropart. Phys.*, **2023**, 004
 Evans M., et al., 2021, arXiv e-prints, p. arXiv:2109.09882
 Fishbach M., Kimball C., Kalogera V., 2022, *ApJ*, **935**, L26
 Franciolini G., Musco I., Pani P., Urbano A., 2022, *Phys. Rev. D*, **106**, 123526
 Hild S., et al., 2011, *Classical and Quantum Gravity*, **28**, 094013
 Isoyama S., Nakano H., Nakamura T., 2018, *PTEP*, **2018**, 073E01
 Kinugawa T., Inayoshi K., Hotokezaka K., Nakauchi D., Nakamura T., 2014, *MNRAS*, **442**, 2963
 Kinugawa T., Nakamura T., Nakano H., 2020, *MNRAS*, **498**, 3946
 Kinugawa T., Nakamura T., Nakano H., 2021a, *MNRAS*, **501**, L49
 Kinugawa T., Nakamura T., Nakano H., 2021b, *MNRAS*, **504**, L28
 Kinugawa T., Nakamura T., Nakano H., 2021c, *Progress of Theoretical and Experimental Physics*, **2021**, 021E01
 Li Y.-J., Wang Y.-Z., Tang S.-P., Yuan Q., Fan Y.-Z., Wei D.-M., 2022, *ApJ*, **933**, L14
 Mahapatra P., Gupta A., Favata M., Arun K. G., Sathyaprakash B. S., 2022, arXiv e-prints, p. arXiv:2209.05766
 Mandel I., Broekgaarden F. S., 2022, *Living Reviews in Relativity*, **25**, 1
 Mandel I., Fragos T., 2020, *ApJ*, **895**, L28
 Marigo P., Girardi L., Chiosi C., Wood P. R., 2001, *A&A*, **371**, 152
 Mould M., Gerosa D., Taylor S. R., 2022a, *Phys. Rev. D*, **106**, 103013
 Mould M., Gerosa D., Broekgaarden F. S., Steinle N., 2022b, *MNRAS*, **517**, 2738
 Nakamura T., et al., 2016, *Progress of Theoretical and Experimental Physics*, **2016**, 093E01
 Oh M., Fishbach M., Kimball C., Kalogera V., Ye C., 2023, *ApJ*, **953**, 152
 Rastello S., Mapelli M., Di Carlo U. N., Iorio G., Ballone A., Giacobbo N., Santoliquido F., Torniamenti S., 2021, *MNRAS*, **507**, 3612
 Santoliquido F., Mapelli M., Iorio G., Costa G., Glover S. C. O., Hartwig T., Klessen R. S., Merli L., 2023, *MNRAS*, **524**, 307
 Seto N., Kawamura S., Nakamura T., 2001, *Phys. Rev. Lett.*, **87**, 221103
 Stegmann J., Antonini F., Schneider F. R. N., Tiwari V., Chattopadhyay D., 2022a, *Phys. Rev. D*, **106**, 023014
 Stegmann J., Antonini F., Moe M., 2022b, *MNRAS*, **516**, 1406
 The LIGO Scientific Collaboration The Virgo Collaboration The KAGRA Scientific Collaboration 2023, The Online Gravitational-wave Transient Catalog (GWTC), <https://gwosc.org/eventapi/html/GWTC/>
 Tiwari V., 2022, *ApJ*, **928**, 155
 Trani A. A., Rastello S., Di Carlo U. N., Santoliquido F., Tanikawa A., Mapelli M., 2022, *MNRAS*, **511**, 1362
 Wagg T., Broekgaarden F. S., de Mink S. E., Frankel N., van Son L. A. C., Justham S., 2022, *ApJ*, **937**, 118
 Zevin M., Berry C. P. L., Coughlin S., Chatziioannou K., Vitale S., 2020, *ApJ*, **899**, L17